



Published in final edited form as:

Cancer Discov. 2015 June ; 5(6): 652–667. doi:10.1158/2159-8290.CD-14-1507.

HIF-2 α dependent lipid storage promotes endoplasmic reticulum homeostasis in clear cell renal cell carcinoma

Bo Qiu^{1,2}, Daniel Ackerman¹, Danielle J. Sanchez^{1,3}, Bo Li¹, Joshua D. Ochocki¹, Alison Grazioli¹, Ekaterina Bobrovnikova-Marjon^{1,*}, J. Alan Diehl⁴, Brian Keith^{1,2}, and M. Celeste Simon^{1,3,5}

¹Abramson Family Cancer Research Institute, Perelman School of Medicine at the University of Pennsylvania, Philadelphia, PA 19104, USA

²Department of Cancer Biology, Perelman School of Medicine at the University of Pennsylvania, Philadelphia, PA 19104, USA

³Department of Cell and Developmental Biology, Perelman School of Medicine at the University of Pennsylvania, Philadelphia, PA 19104, USA

⁴Department of Biochemistry and Molecular Biology, Medical University of South Carolina, Charleston, SC 29425, USA

⁵Howard Hughes Medical Institute

Abstract

Two hallmarks of clear cell renal cell carcinoma (ccRCC) are constitutive hypoxia inducible factor (HIF) signaling and abundant intracellular lipid droplets (LDs). However, regulation of lipid storage and its role in ccRCC are incompletely understood. Transcriptional profiling of primary ccRCC samples revealed that expression of the LD coat protein gene *PLIN2* was elevated in tumors and correlated with HIF-2 α , but not HIF-1 α , activation. HIF-2 α dependent *PLIN2* expression promoted lipid storage, proliferation, and viability in xenograft tumors.

Mechanistically, lipid storage maintained integrity of the endoplasmic reticulum (ER), which is functionally and physically associated with LDs. Specifically, *PLIN2* dependent lipid storage suppressed cytotoxic ER stress responses that otherwise result from elevated protein synthetic activity characteristic of ccRCC cells. Thus, in addition to promoting ccRCC proliferation and anabolic metabolism, HIF-2 α modulates lipid storage to sustain ER homeostasis, particularly under conditions of nutrient and oxygen limitation, thereby promoting tumor cell survival.

Keywords

HIF-2 α ; lipid storage; lipid droplets; clear cell renal cell carcinoma; ER stress

Corresponding Author: M. Celeste Simon, Ph.D, Rm 456 BRB II/III, 421 Curie Blvd, Philadelphia, PA 19104, Phone: (215) 746-5532, Facsimile: (215) 746-5511, celeste2@mail.med.upenn.edu.

*Present address: Agios Pharmaceuticals, Cambridge, MA 02139

Conflicts of Interest: The authors have no conflicts of interest to report.

Introduction

Clear cell renal cell carcinoma (ccRCC) is the most common form of kidney cancer worldwide (1, 2). In 90% of ccRCC tumors, pathogenesis is characterized by constitutive activation of the hypoxia inducible factors (HIFs) due to loss of the pVHL (*von Hippel-Lindau*) tumor suppressor, required for oxygen (O₂) dependent suppression of HIF signaling (1). HIF regulated processes are orchestrated by two HIF- α subunits (HIF-1 α and HIF-2 α), which share several common transcriptional targets, but also exhibit distinct functions (2). This is particularly evident in ccRCC, where HIF-1 α expression is frequently lost during disease progression, and pre-clinical data indicate that it can repress tumor growth (3). The central role of HIF-2 α in ccRCC is supported by findings that 1) all pVHL-null ccRCC maintain HIF-2 α expression (4), 2) HIF-2 α function is required for ccRCC xenograft growth (1, 2), and 3) polymorphisms in *EPAS1/HIF2 α* are associated with increased ccRCC risk in GWAS studies (5). HIF-dependent gene expression contributes directly to enhanced cell proliferation (6) and metabolic alterations that characterize ccRCC (1, 7).

A second hallmark of ccRCC is the presence of intracellular lipid droplets (LDs), which consist of a neutral lipid core containing triglycerides and cholesterol-esters surrounded by a phospholipid monolayer and associated LD surface proteins (8). Two well-characterized functions of lipid storage in eukaryotic cells include energy homeostasis and release of lipid species for membrane synthesis during proliferation (8). In addition, LDs are functionally and physically associated with the endoplasmic reticulum (ER), as lipids and the proteins that synthesize/modify them are exchanged between these organelles via transient membrane bridges (9). The PAT (Perilipin, Adipophilin, Tip47) family of LD coat proteins regulate both lipid storage and lipolysis (8). Perilipin (*PLIN1*) is expressed primarily in adipose and steroidogenic cells, while Adipophilin/Adipose Differentiation Related Protein (hereafter referred to as Perilipin 2, *PLIN2*) and TIP47 (*PLIN3*) are ubiquitously expressed and function as the predominant LD coat proteins in non-adipose tissue (10). Interestingly, *PLIN2* expression is positively correlated with HIF-2 α activation in mouse hepatocytes *in vivo* (11), and our microarray data suggest that HIF-2 α promotes *PLIN2* mRNA expression in ccRCC cells *in vitro* (12). However, it remains unknown if *PLIN2* regulates lipid metabolism and storage downstream of HIF-2 α or if this phenotype has any significant tumor-promoting functions in ccRCC.

Enhanced lipid storage in ccRCC suggests profoundly altered lipid metabolism. In normal cells, lipid metabolism is carefully regulated to support membrane expansion, organelle homeostasis, signal transduction, and cell viability. Recent work indicates that cellular transformation commits tumors to growth programs that strain ER homeostasis, including dysregulation of protein and lipid metabolism (13). Such ER stress is exacerbated by conditions of nutrient and O₂ deprivation characteristic of solid tumor microenvironments, which further disrupt cellular protein and lipid homeostasis (14). Mammalian cells activate a highly conserved unfolded protein response (UPR) upon elevated mis-folded protein load or disruption of ER membrane lipid composition (15). ER stress sensors, including PERK, IRE-1 α , and ATF6, initiate UPR signaling and adaptive processes, including a generalized reduction in protein synthesis and selective expression of genes encoding lipid synthetic enzymes, protein-folding chaperones, and components of the ER associated degradation

(ERAD) system for enhancing proteasome dependent proteolysis (15). However, sustained and irremediable ER stress can trigger cell death via a “terminal” UPR (16). Indeed, anti-tumor activity of the proteasome inhibitor Bortezomib in multiple myeloma derives at least partly from elevated mis-folded protein levels and induction of a cytotoxic UPR (17).

In this study, we explored mechanisms that regulate lipid storage and its function in ccRCC. Transcriptional profiling of primary ccRCC and normal kidney samples revealed that *PLIN2*, but not other perilipin family members, is overexpressed in ccRCC and positively correlated with HIF-2 α activation. HIF-2 α promoted *PLIN2* expression and lipid storage in ccRCC cell lines, and remarkably, *PLIN2* activity accounted for a substantial portion of HIF-2 α 's tumor-promoting effects in xenograft assays. Mechanistically, the HIF-2 α /*PLIN2*/lipid storage axis was required for ER homeostasis and resistance against cytotoxic ER stress. These findings reveal an unexpected function for the “clear cell” phenotype and identify enhanced ER stress as a targetable vulnerability created by HIF-2 α suppression in ccRCC.

Results

***PLIN2* is overexpressed in ccRCC patient samples and positively correlated with HIF-2 α activation**

To confirm the contribution of neutral lipid storage to the “clear cell” phenotype in our archived ccRCC tissues, we performed oil red O staining of primary tumor and matched normal kidney samples and observed enhanced neutral lipid staining in ccRCC tumor cells (Fig. 1A). Potential mediators of enhanced lipid storage were identified by analyzing RNA-seq data released by The Cancer Genome Atlas (TCGA) comparing primary ccRCC (n=480) and normal kidney (n=69) tissues (18). Focusing on expression of the PAT family of lipid droplet coat proteins, we observed that *PLIN2* was overexpressed in tumors across all stages of disease (Fig. 1B). In contrast, mRNA expression of other perilipin family members was not enhanced in ccRCC (Fig. S1A). *PLIN2* upregulation was confirmed in an independent set of matched ccRCC (n=10) and normal kidneys (n=10) from our archived samples (Fig. 1C). Analysis of “Triglyceride Synthesis” and “Cholesterol Synthesis” gene-sets within the TCGA RNA-seq dataset, as defined by the Broad Institute Molecular Signatures database, revealed differential expression of many lipogenic genes (Tables S1–2). Some fatty acid and triglyceride synthesis genes were upregulated within tumor tissues (i.e. *ACLY*, *ELOVL2*, *LPCAT1*), while many others were downregulated (i.e. multiple *ACSL* and *AGPAT* family members) (Table S1). On the other hand, the expression of most cholesterol biosynthetic enzymes was decreased in tumor tissue relative to normal kidney (Table S2). Although altered expression of triglyceride and cholesterol synthesis enzymes may impact lipid synthesis and storage in ccRCC, we focused our attention on *PLIN2* for multiple reasons. First of all, functional studies in murine models of hepatosteatosis have revealed that *Plin2* upregulation is necessary for lipid storage and enhanced *de novo* lipid synthesis, even if other lipogenic genes were overexpressed (i.e. *Elovl3*, *Fasn*, *Scd1*) (19, 20). Secondly, overexpression of *Plin2* alone was sufficient to drive lipid synthesis and storage in murine liver (19) and mouse embryonic fibroblasts (21). Taken together with the observation that HIF-2 α activation and *PLIN2* expression are positively correlated in various settings (11,

22), these findings suggested a functional connection between two hallmarks of ccRCC—constitutive HIF activity and heightened neutral lipid storage.

Analysis of microarray data profiling gene expression in normal kidney and distinct renal malignancies (23) revealed that *PLIN2*, along with a panel of established HIF-2 α target genes, is specifically elevated in ccRCC samples (Fig. S1B). Because pVHL loss of function is a defining feature of most ccRCC, we examined whether HIF activation promotes *PLIN2* expression. To explore this link in ccRCC patient samples, we performed transcriptome profiling of tumors previously grouped into three categories based on HIF- α staining and *VHL* gene sequencing: *VHL* WT (no HIF- α staining), HIF-1 α and HIF-2 α expressing (“H1H2”), and HIF-2 α only (“H2”) (4). This analysis indicated that *PLIN2* mRNA was elevated in both H1H2 (9.7 fold overexpression, $p=2.6E4$) and H2 (16.7 fold overexpression, $p=2.5E-6$) tumors when compared to *VHL* WT samples (Fig. 1D). Multiple documented HIF-2 α targets in ccRCC exhibited a similar expression pattern (Fig. 1D). Collectively, these observations suggest that *PLIN2* levels increase early in disease progression and correlate with enhanced HIF-2 α activity in ccRCC patient samples.

To directly examine the role of HIF-2 α in *PLIN2* regulation in ccRCC, we depleted HIF-2 α from 786-O (H2) and RCC4 (H1H2) ccRCC cell lines using multiple shRNAs and found that *PLIN2* mRNA and protein expression was reduced (Fig. 1E–F). In contrast, *HIF1A* silencing in RCC4 cells actually enhanced *PLIN2* mRNA and protein levels, while decreasing levels of the HIF-1 α target pyruvate dehydrogenase kinase 1 (*PDK1*) (Fig. 1F). These results are consistent with the *PLIN2* expression pattern we observed in primary patient samples (Fig. 1D). We also determined whether peroxisome proliferator-activated receptor gamma (PPAR γ) regulates *PLIN2* in ccRCC, as PPAR γ is overexpressed in ccRCC tissue and was previously shown to stimulate *PLIN2* transcription in the settings of hepatosteatosis and foam cell formation (24). In A498 cells, which exhibit high levels of both PPAR γ and *PLIN2*, *PPARG* shRNAs reduced PPAR-response element reporter activity, but not *PLIN2* levels (Fig. S2A–B). PPAR α (*PPARA*) also promotes *PLIN2* transcription in states of lipid accumulation (10). However, expression of *PPARA* and many of its target genes are reduced in ccRCC compared to normal kidney tissue (Fig. S2C–D), decreasing the likelihood that it regulates *PLIN2* in ccRCC. These findings suggest that constitutive HIF-2 α activity, rather than PPAR γ , PPAR α , or HIF-1 α , regulates *PLIN2* in both ccRCC cell lines and primary patient samples.

HIF-2 α /PLIN2 promote lipid storage and tumor growth in ccRCC xenografts

PLIN2 is commonly used as a marker of cellular lipid accumulation, but its overexpression is also sufficient to increase lipid synthesis and storage in murine fibroblasts *in vitro* (21) and liver *in vivo* (19). Given the numerous tumor-promoting processes downstream of HIF-2 α , we tested whether *PLIN2* restoration alone was sufficient for tumor growth following HIF-2 α suppression in multiple model systems. Doxycycline (Dox)-inducible shRNA was used to deplete HIF-2 α in 786-O cells constitutively expressing either pCDH empty vector (EV) or an exogenous *PLIN2* cDNA. Xenografts generated from these two cell lines grew at identical rates prior to Dox exposure (data not shown). After administration of Dox-chow to inhibit HIF-2 α , EV xenografts exhibited a steady decline in tumor volume and

reduced mass at sacrifice, whereas those expressing exogenous PLIN2 demonstrated partial maintenance of both tumor volume and mass (Fig. 2A, left and center). qRT-PCR analysis confirmed that HIF-2 α regulates *PLIN2* *in vivo* and exogenous *PLIN2* mRNA levels were maintained following Dox-induced HIF-2 α depletion (Fig. 2A, right). Furthermore, oil red O staining indicated that HIF-2 α loss reduced neutral lipid staining, whereas exogenous PLIN2 fully restored lipid storage (Fig. 2B–C). These results indicate that PLIN2 is both necessary and sufficient to promote neutral lipid storage in ccRCC xenografts. Further histological analysis revealed that HIF-2 α depletion dramatically decreased tumor cell proliferation, as indicated by Ki67 staining, which was partially restored by exogenous PLIN2 (Fig. 2B–C). We also found that HIF-2 α suppression resulted in large areas of tissue necrosis and induction of apoptosis, based on cleaved caspase 3 accumulation, which were both reduced by *PLIN2* expression (Fig. 2B–C).

Despite the complexity of HIF-2 α dependent tumorigenesis *in vivo*, including cell extrinsic effects such as angiogenesis, PLIN2 restoration alone significantly restored tumor cell proliferation and viability. We reasoned that enhanced lipid storage imparts a cell intrinsic advantage to tumor cells. To test this hypothesis, we generated *in vitro* 3D tumor spheroids using 786-O cells, which recapitulate nutrient and O₂ gradients within solid tumors (Fig. S3A). In this assay, HIF-2 α inhibition was associated with loss of neutral lipid staining and enhanced cell death, while exogenous PLIN2 expression partially restored lipid storage and reduced cell death (Fig. S3B–C). Thus, multiple tumor model systems suggest an essential role for PLIN2 dependent lipid storage downstream of HIF-2 α in ccRCC.

PLIN2 dependent lipid storage is required for ER homeostasis and cell viability in ccRCC cell lines and xenograft tumors

The finding that PLIN2 is required for cell viability in ccRCC xenografts was surprising, as acute *PLIN2* depletion experiments have reported no effects on cell viability either *in vivo* or *in vitro* (19, 20, 25). To assess the effects of direct PLIN2 depletion in ccRCC, we expressed multiple shRNAs targeting *PLIN2* or a scrambled control (SCR) in 786-O and A498 cells. In both cell lines, we observed a dosage dependent loss of cell viability and proliferation that correlated with degree of *PLIN2* depletion (Fig. 3A–B; S4A–B). Oil red O staining and BODIPY 493/503 quantification also revealed dosage dependent decreases in neutral lipid levels (Fig. 3C–D). To assess functional lipid storage capacity, cells were treated with oleic acid, a potent inducer of triglyceride synthesis and neutral lipid storage that is selectively toxic for cells incapable of storing it as triglyceride (26). Consistent with decreased ability to store lipids within LDs, *PLIN2* depleted cells were preferentially sensitized to oleic acid induced cell death (Fig. 3E).

In light of the intimate ER/LD relationship and evidence that altered membrane properties can trigger ER stress (13, 15), we reasoned that decreased lipid storage capacity could disrupt ER homeostasis and trigger the UPR, cell cycle withdrawal, and cell death. PLIN2 ablation in 786-O cells elicited dosage dependent activation of UPR sensors PERK, IRE-1 α , and ATF6 and induction of multiple UPR target genes (Fig. 4A). Furthermore, ER Tracker imaging and flow cytometry indicated ER expansion in PLIN2 depleted cells (Fig. 4B) and ultra-structural analysis by transmission electron microscopy (TEM) confirmed the presence

of dilated and irregularly shaped rough ER (Fig. 4C), both of which are consistent with ER stress (27). Similarly, PLIN2 depletion in A498 cells elicited morphological and gene expression changes indicative of ER stress (Fig. S4C–D). Based on these observations, we quantified UPR target gene expression in HIF-2 α deficient xenograft tumors. Indeed, multiple UPR targets, including the “terminal” UPR genes *CHOP* and *TXNIP*, were elevated in HIF-2 α depleted tumors and decreased by exogenous *PLIN2* expression (Fig. 4D).

To determine if UPR activation promotes cell death upon PLIN2 loss in ccRCC, we utilized previously characterized small molecule PERK and IRE-1 α inhibitors, along with siRNA against *ATF6*, to suppress UPR signaling (28, 29). These tools were validated in A498 cells, based on UPR sensor phosphorylation status and target gene expression (Fig. S5A–D). In 786-O cells, PERK inhibition reduced *ATF3* levels (a PERK/ATF4 target) in *PLIN2* depleted cells, but enhanced cell death and expression of multiple IRE-1 α and ATF6 target genes (Fig. 5A; S5B–D). Whereas IRE-1 α and ATF6 suppression each modestly restored cell viability, combined suppression of both yielded enhanced cell survival (Fig. 5B). In A498 cells, ATF6 promoted cell death downstream of PLIN2 inhibition (Fig. S6A–B). While the specific UPR-sensor(s) mediating cell death varies between cell lines, our results indicate that PLIN2 is required for maintenance of ER homeostasis and prevention of cytotoxic ER stress in ccRCC. Next, we examined the potential sources of ER stress that could explain the enhanced requirement for PLIN2-mediated ER homeostasis in ccRCC.

PLIN2 dependent lipid storage supports ER homeostasis during oncogene mediated activation of protein synthesis

The observation that ccRCC cells require PLIN2 for proliferation and viability was surprising, because 1) *Plin2* knockout mice are viable (30), 2) *Plin2* deficient macrophages do not exhibit enhanced sensitivity to cholesterol loading, which requires lipid storage to alleviate ER stress (31), and 3) acute *Plin2* suppression fails to elicit cell death in steatotic hepatocytes (19, 20), MCF7 breast cancer cells, or U87 glioblastoma cells (25). One potential advantage of lipid storage in ccRCC is the ability to derive energy from fatty acid breakdown via β -oxidation. However, in contrast to the electron transport chain inhibitor rotenone, PLIN2 depletion did not affect ATP levels in multiple ccRCC cell lines (Fig. S7A). Furthermore, transcription factors that promote renal tubular cell β -oxidation, including *PPARA* and PPAR γ coactivator 1-alpha (*PPARGC1A*), were substantially downregulated in primary ccRCCs compared to normal kidney (Fig. S2C, S7B). The Carnitine/Acyl-carnitine Transporter (*CAT*) and mitochondrial β -oxidation enzymes were also underexpressed in ccRCC tissues (Fig. S7B, C). In agreement with these findings, metabolomic analysis of primary ccRCC and normal kidney tissues revealed elevation of acyl-carnitine levels in tumors (Table S3). These features of ccRCC mirror genetic *CAT* deficiency, which manifests as acyl-carnitine build up secondary to reduced β -oxidation flux (32). Furthermore, a recent study indicates that HIF-2 α suppresses peroxisomal β -oxidation via selective autophagy of peroxisomes (33). Thus, alterations to β -oxidation are unlikely to explain the effects of PLIN2 depletion in ccRCC.

Next, we explored whether enhanced tumor anabolic processes, downstream of oncogenic activation, contribute to the requirement for PLIN2 dependent lipid storage in ccRCC.

Particularly, increased protein and lipid synthesis via mTORC1 could result in a greater requirement for lipid storage to maintain ER homeostasis, as the ER functions as a “hub” for both protein and lipid production. We focused on mTORC1 because 1) 30% of ccRCC harbor activating mutations in the mTOR pathway (18), 2) most tumors exhibit elevated mTORC1 activity (p-S6K1, p4EBP1 staining) (4, 34), and 3) mTORC1 can stimulate both protein and lipid synthesis (35, 36). The effects of small molecule mTOR inhibitors on protein and lipid synthesis were characterized in ccRCC cells. As expected (35), Torin1 was more potent than rapamycin in suppressing protein synthesis and lipogenic enzyme gene expression in ccRCC cells (Fig. 6A–B). In both 786-O and A498 cells, rapamycin and Torin1 treatment enhanced viability and reduced UPR gene expression following PLIN2 depletion, with Torin1 being more potent (Fig. 6C; S8A–B). Notably, the magnitude of restored viability upon mTOR suppression was greater than that observed upon UPR inhibition in both 786-O and A498 cells (Fig. 5A–B, 6C; S8B). We reasoned that this was due to amelioration of ER stress, rather than merely UPR signaling itself.

Given that Torin1 suppresses both protein and lipid synthesis, we measured the relative contribution of these activities toward Torin1 dependent effects. Suppression of protein synthesis using the translation inhibitor cycloheximide (CHX) restored cell viability and ameliorated ER stress in PLIN2 depleted cells (Fig. 6D–E). On the other hand, silencing of sterol regulatory element-binding proteins 1 and 2 (SREBP1/2), mediators of lipid synthesis downstream of mTORC1 (35), selectively reduced viability in PLIN2 depleted cells (Fig. S8C–D). Consistent with an adaptive function of SREBP1/2 activation in cells experiencing ER stress (16, 37), PLIN2 depletion induced multiple lipid synthesis enzymes in an SREBP1/2-dependent manner (Fig. S8C–D). Ultimately, CHX treatment restored cell viability in PLIN2 depleted cells, even when SREBP1 and 2 were inhibited, reflecting the aggregate activities of Torin1 (Fig. S8C–D). These findings suggest that protein synthesis is a prominent source of ER stress and cell death in the setting of PLIN2 depletion.

HIF-2 α dependent PLIN2 expression and lipid storage promote resistance against pharmacologic ER stress

Given that reduction of ER protein load alleviated ER stress in PLIN2 depleted cells, we determined if such cells would also be more sensitive to agents that increase mis-folded protein load. Of note, PLIN2 depleted cells were more sensitive to tunicamycin treatment, which inhibits N-linked glycosylation, compared to controls (Fig. 7A). We performed similar experiments to determine if HIF-2 α /PLIN2 mediated lipid storage is similarly protective against pharmacological ER stress. A498 cells expressing *HIF2A* shRNA exhibited reduced BODIPY staining, whereas exogenous PLIN2 expression was sufficient to restore neutral lipid levels (Fig. 7B). Upon treatment with tunicamycin, HIF-2 α depleted cells exhibited a 3-fold enhancement of cell death that was partially ameliorated by restoring PLIN2 dependent lipid storage (Fig. 7C). Treatment with brefeldin A, an ER stress inducing agent that inhibits ER to golgi vesicular transport, yielded consistent results (Fig. S9A–B).

PLIN2 also protected ccRCC cells from the proteasome inhibitor Bortezomib (Fig. 7D), an FDA approved therapy for multiple myeloma that functions partly through ER stress induction (17). Specifically, expression of the IRE-1 α substrate spliced *XBPI* is positively

correlated with patient response to Bortezomib and functional studies demonstrate a role for the UPR target gene *CHOP* in Bortezomib-mediated cell death (38, 39). Consistent with a cytotoxic function of ER stress in Bortezomib treated ccRCC cells, the enhanced efficacy of Bortezomib in *PLIN2* depleted cells was associated with elevated levels of spliced *XBP1* and *CHOP* (Fig. 7E). Furthermore, HIF-2 α depleted cells demonstrated enhanced sensitivity to Bortezomib that was ameliorated by exogenous *PLIN2* (Fig. 7F). Next, we tested whether nutrient and/or O₂ deprivation—ER stress inducing conditions found within the tumor microenvironment (13)—could further enhance Bortezomib-induced cell death. Indeed, previous work indicates that hypoxia can enhance anti-tumor activity of Bortezomib via ER stress induction (40). Growth under conditions of serum and/or O₂ deprivation enhanced Bortezomib induced cell death, most prominently in *PLIN2* depleted cells (Fig. 7G). Under each condition tested, expression of the terminal UPR gene *CHOP* was also positively correlated with degree of cell death (Fig. S9C).

Collectively, we suggest a model in which HIF-2 α /*PLIN2* dependent lipid storage promotes ER homeostasis and prevents cytotoxic ER stress in ccRCC cells (Fig. 7H). This phenotype promotes cell viability under multiple conditions that perturb ER homeostasis, including growth under limited nutrient/O₂ delivery within solid tumors, enhanced protein synthesis downstream of oncogenic activation, and exposure to pharmacological ER stress inducing drugs.

Discussion

Despite the longstanding observation that ccRCC tumor cells exhibit abundant intracellular LDs, a clear function for this phenotype had not been identified. In this study, we explored the role of LD coat proteins in ccRCC progression. Analysis of multiple cohorts of primary ccRCC patient samples revealed *PLIN2* overexpression in tumor samples and suggested a functional relationship between pVHL loss, constitutive HIF-2 α activation, and *PLIN2* accumulation. While previous reports indicated that *PLIN2* expression and lipid storage correlated with HIF-2 α activation, it was unknown whether *PLIN2* was a driver of this phenotype, or a passenger of broader metabolic changes (11). Our findings indicate that *PLIN2* is both necessary and sufficient to promote lipid storage in ccRCC cell lines. Mechanistically, HIF-2 α dependent *PLIN2* expression and lipid storage is required for maintenance of ER homeostasis and prevention of cytotoxic ER stress.

The significant requirement for *PLIN2* in ccRCC cells was intriguing, as *Plin2* $-/-$ mice are viable and acute *PLIN2* depletion studies in settings of lipid accumulation (i.e. hepatosteatosis or foam cell formation) have reported no evidence of ER stress or cell death (30, 31, 41). We provide two potential explanations for this observation. First of all, in physiological scenarios, PPAR family members coordinately enhance expression of *PLIN2* and other PAT LD coat proteins (10). In these settings, *PLIN2* loss of function is associated with compensatory upregulation of other LD coat proteins (30, 41). However, we determined that *PLIN2* is upregulated in ccRCC due to HIF-2 α activation, rather than by PPAR γ or PPAR α . Moreover, *PLIN2* is overexpressed independently of other PAT LD coat proteins in ccRCC, likely explaining why functional compensation cannot be achieved after *PLIN2* depletion. Secondly, our results suggest that an enhanced requirement for *PLIN2*

dependent lipid storage and ER homeostasis could arise from heightened ER stress downstream of oncogene activation. These include cell intrinsic stress from enhanced protein synthesis and cell extrinsic stress due to commitment to a growth rate that outstrips nutrient and O₂ delivery.

Our results fit within an emerging theme in which oncogenic transformation coordinately induces both anabolic processes to increase proliferation and homeostatic pathways that maintain cell viability. These include proteasome activity downstream of mTORC1, autophagy downstream of MYC overexpression (42), and lipid/protein scavenging by RAS transformed tumors (43, 44). Thus, different oncogenes appear to solve the problem of balancing proliferation and cellular homeostasis in unique ways. In the case of ccRCC, we suggest a model in which HIF-2 α dependent lipid storage occurs early in disease progression and functions to buffer tumor cells against cell intrinsic and extrinsic sources of ER stress. In ccRCC, the heightened proliferation and anabolic metabolism is driven by HIF-2 α dependent processes such as autocrine growth factor signaling via TGF α and VEGFA, mTORC1 stimulation, and cell cycle progression, and independent oncogenic events that activate mitogenic pathways (6, 18, 45). Although enhanced lipid storage is a hallmark feature of ccRCC, this phenotype is observed in other malignancies, including Burkitts lymphoma, hepatocellular carcinoma, and advanced prostate cancer (46, 47). While the underlying mechanisms of lipid storage and the function it serves may vary between cancer types, additional studies into the role of lipid storage in cancer are warranted.

Our results indicate that heightened protein synthesis is a prominent source of ER stress in PLIN2 deficient ccRCC cells. While the initial perturbation to ER homeostasis in such cells is likely due to alterations in ER lipid content, the cumulative level of ER stress likely arises from dysregulation of both protein and lipid metabolism, which independently trigger the UPR (14). In addition, disruption of ER lipid composition can further impair protein-folding capacity and enhance ER stress (48). Mechanistically, PLIN2 promotes neutral lipid content through at least two, non-mutually exclusive, mechanisms: enhancing lipid storage and suppressing lipolysis. Our observation that oleic acid is selectively toxic to PLIN2 depleted cells suggests that at least a portion of the PLIN2 deficient phenotype arises from loss of the ability to package lipids into LDs. This phenotype is also observed in mouse embryonic fibroblasts that are deficient in enzymes (diacylglyceride-acyltransferases, DGATs) that are required to incorporate oleic acid into triglycerides (26). However, it remains to be tested how PLIN2 affects lipolysis in ccRCC. Additionally, future studies that characterize the specific changes in ER lipid composition following PLIN2 depletion may provide additional strategies to enhance tumor cell ER stress.

Lastly, our finding that loss of HIF-2 α /PLIN2 dependent lipid storage enhances sensitivity to ER stress inducing agents has implications for ccRCC therapy. A therapeutic index has previously been demonstrated for the proteasome inhibitor Bortezomib in multiple myeloma, where heightened immunoglobulin synthesis within ER renders cells more sensitive to pharmacological ER stress (17). A small phase II clinical trial evaluating Bortezomib mono-therapy for advanced renal cancer revealed partial responses in only 12% (3/25) of ccRCC patients (49). HIF-2 α /PLIN2 dependent lipid storage and ER stress resistance could contribute to this limited response rate. Specifically, our observation that

multiple components of the ERAD machinery (*HERP*, *HRD1*, *ERdj4*) were induced in HIF-2 α depleted tumors provides initial evidence for the rational combination of proteasome inhibitors and HIF-2 α suppression, especially as HIF-2 α specific inhibitors are currently under development for treatment of ccRCC (Clinical Trial No. NCT02293980).

Methods

Primary patient samples

Fresh frozen ccRCC or matched normal kidney patient samples were obtained from the Cooperative Human Tissue Network (CHTN). Samples were de-identified and handled in accordance with institutional review boards.

Cell Culture and viability assays

Authenticated (short tandem repeat profiling) human ccRCC cell lines 786-O, A498, and RCC4 were obtained from the American Type Culture Collection in 2001. Cells were cultured for a maximum of four weeks before thawing fresh, early passage cells. All cells were confirmed to be mycoplasma negative (MycoAlert, tested June 2014) and verified for pVHL and HIF α expression status using western blot analysis. Cells were cultured in Dulbecco's Modified Eagle Medium (DMEM) + 10% FBS. Cell viability was determined using the FITC-Annexin V, PI kit (Cat 556547) from BD Biosciences according to the manufacturer's instructions. Flow cytometry was performed using the BD Accuri C6 instrument and double negative cells were deemed viable.

3D spheroid cultures were generated using the liquid overlay technique. 24 well plates were coated with 1% agarose in DMEM prior to plating 100,000 cells per well in DMEM + 10% FBS. To promote spheroid formation, plates were swirled prior to incubation. Media was changed every 3 days and spheroids were harvested after 9 days. Hypoxic cells were labeled by incubating spheroids with 200 μ M FITC-conjugated pimonidazole hydrochloride (Hypoxyprobe, Cat HP2) prior to fixation. For BODIPY 493/503 quantification, spheroids were dissociated with Accutase at 37°C for 30 minutes and stained as described below in "BODIPY staining".

Reagents

Oleic Acid (Cat O3008), rapamycin (Cat R8781), tunicamycin (Cat T7765), and brefeldin A (Cat B7651) were purchased from Sigma Aldrich. GSK2656157 PERK inhibitor (Cat 5046510001), 4 μ 8C IRE-1 α inhibitor (Cat 412512), Torin1 (Cat 475991), and cycloheximide (Cat 239763) were purchased from Millipore. siRNA pools targeting human *ATF6* (Cat L-009917), *SREBF1* (Cat L-006891), and *SREBF2* (Cat L-009549) were purchased from Dharmacon. Rotenone (Cat 557368) was purchased from EMD Chemicals. Bortezomib was purchased from Cell Signaling Technologies (Cat 2204S).

Plasmids, lentivirus production, and viral transduction

The lentiviral vector PLKO.1 SCR (Plasmid No. 17920) was obtained from Addgene. pLKO.1 vectors expressing shHIF1A_9 (TRCN0000003809), shHIF2A_6 (TRCN0000003806), shHIFA_7 (TRCN0000003807), shPLIN2_1 (TRCN0000136605),

shPLIN2_2 (TRCN0000136481), shPPARG_2 (TRCN0000001672), and shPPARG_3 (TRCN0000001673) were obtained from the Broad Institute TRC shRNA library. The GIPZ vector expressing shHIF1A_52 (V3LMM_441752) was obtained from Dharmacon. PLIN2 open reading frame was sub-cloned from MGC sequence verified cDNA (Dharmacon, Clone ID: 3844174) into the PCDH-CMV-MCS-EF1-HYGRO mammalian expression vector. The Doxycycline inducible shHIF2A_7 construct was generated using the “Tet-pLKO-puro” plasmid (Addgene Cat 21915).

Lentivirus was produced by transfecting 293T cells with the indicated expression plasmid, pRSV-Rev, pMDL, and pCMV-VSV-G plasmids using Fugene6 (Promega). Virus was harvested 48 hours after transfection. For viral infection, cells were incubated with medium containing virus and 8µg/ml polybrene for 16 hours. Cells were allowed to recover for 48 hours before antibiotic selection, and surviving pools were utilized for downstream analyses.

Xenografts

Sub-cutaneous xenograft experiments were approved by the Animal Care and Use Committee at the University of Pennsylvania. NIH-III nude mice (Charles River, 4–6 weeks old) were injected in each flank with five million cells in a 1:1 mixture of PBS and Matrigel (BD 356234). Tumor volume was monitored by caliper measurements. After tumors reached 300mm³, mice were split into cohorts receiving standard chow or Doxycycline chow (625 mg/kg, Harlan Labs Cat TD05125) *ad libitum*. After 11 days on the indicated chow, animals were sacrificed by CO₂ inhalation and xenograft tumors were dissected for downstream analyses.

TCGA RNA-seq analysis

Level 3 RNA-seq data for 480 ccRCC and 69 normal kidney samples was downloaded from the TCGA on April 2, 2013. Differential gene expression analysis of tumor and normal samples was performed using DeSeq (Bioconductor Version 2.12). Box and whisker plots correspond to 1–99th percentiles (bars), 25–75th percentiles (box), and median (line in box). Differentially expressed genes were subjected to gene set enrichment analysis (GSEA) using the Broad Institute Molecular Signature Database.

Microarray analyses

Classification of primary ccRCC samples into *VHL* WT, H1H2, and H2 sub-groups and microarray analysis is described in Gordan et al (4). Expression data is deposited at the NCBI Gene Expression Omnibus (GEO) under GSE11904. Expression analysis comparing normal kidney, ccRCC, papillary RCC, and chromophobe RCC was described in Jones et al (23). Data was downloaded from GEO (GSE15641).

Tissue staining and imaging

For frozen patient samples, OCT embedded tissue was cut to 10µm sections and fixed in 4% paraformaldehyde (PFA) prior to staining. For xenograft tumors, samples were fixed in 4% PFA, equilibrated in 30% w/v sucrose, and embedded in OCT. 10µm sections were cut for staining. H&E staining was performed as previously described (4).

Oil Red O—A working oil red O solution was generated by diluting a 3.5mg/ml stock (in 100% isopropanol) 6:4 with distilled water. This solution was incubated at room temperature for 30 minutes and filtered in Whatman paper before use. Tissue sections were incubated in 60% isopropanol for 5 minutes, dried at room temperature, and incubated in oil red O staining solution for 1 hour at room temperature. Slides were rinsed in distilled water and counterstained with hematoxylin prior to mounting in Prolong Gold Antifade with DAPI (Life Technologies, Cat P36935).

Immunohistochemistry—Slides were treated in 1% hydrogen peroxide for 30 minutes and blocked in 2% normal goat serum and 4% BSA in Tris buffer with Tween 20. Avidin/Biotin blocking was performed and sections were incubated with primary antibodies overnight at 4°C. Ki67 antibody was used at 1:100 (BD, Cat 550609). Cleaved caspase 3 (Asp175) antibody was used at 1:400 (Cell Signaling, Cat 9661). Slides were incubated in 1:200 dilutions of biotinylated goat anti-mouse (Vector Labs, Cat BA-9200) or anti-rabbit (Vector Labs, Cat BA-1000) secondary antibodies for 1 hour at room temperature. Sections were then processed using the Vectastain Elite ABC kit (Vector Labs, PK-6100) and DAB peroxidase substrate kit (Vector Labs, Cat SK-4100), dehydrated in a standard ethanol/xylenes series, and mounted in 75% v/v Permount (Fischer, Cat SP15-500) in xylenes.

Immunofluorescence—Slides were incubated in 50mM ammonium chloride for 10 minutes, permeabilized with 0.25% Triton X-100 for 10 minutes, and blocked in 2% normal goat serum and 4% BSA for 1 hour. Slides were incubated with cleaved caspase 3 (Asp175) antibody at 1:400 (Cell Signaling, Cat 9661) overnight at 4°C. Secondary Alexa Fluor 488 goat anti-rabbit (Life technologies, Cat A-11008) was used at 1:200 for 1 hour at room temperature. Slides were mounted in Prolong Gold Antifade with DAPI before imaging.

RNA reverse transcription and quantitative RT-PCR analysis

Total RNA was isolated using the RNAeasy purification kit (Qiagen). cDNA was synthesized using the Applied Biosystems High Capacity RNA-to-cDNA master mix. qRT-PCR was performed on a ViiA7 Real Time PCR systems from Applied Biosystems. Pre-designed Taqman primers were obtained from Life Technologies for the following genes: *TBP* (HS01060665_G1), *ACTB* (HS01060665_G1), *VEGFA* (HS00900055_M1), *PLIN2* (HS00605340_M1), *HIF2A/EPAS1* (HS01026149_M1), *HIF1A* (HS00153153_M1), *TGFA* (HS00608187_M1), *PDK1* (HS01561850_M1), *PLIN3* (HS00998416_M1), *BiP/HSPA5* (HS00946084_G1), *XBPI(spliced)* (HS03929085_G1), *CHOP/DDIT3* (HS00358796_G1), *ERO1A/ERO1L* (HS00205880_M1), *HERP/HERPUD1* (HS01124269_M1), *EDEMI* (HS00976004_M1), *ERdj4/DNAJB9* (HS01052402_M1), and *HRD1/SVNI* (HS00381211_M1), and *ATF6* (HS00232586_M1). SYBR-green primers were utilized for human *ATF3* (Forward: TAGGCTGGAAGAGCCAAAGA, Reverse: TTCTCACAGCTGCAAACACC).

BODIPY 493/503 and ER tracker staining

BODIPY 493/503 (Cat D3922) was purchased from Life Technologies. Live cells were washed twice in PBS and incubated in 2µg/ml BODIPY in PBS for 15 minutes at 37°C. After staining, cells were washed twice in PBS and fixed in 2% PFA for 15 minutes. Fixed

cells were washed and re-suspended in PBS, passed through a cell strainer, and analyzed on an Accuri C6 flow cytometer under FL-1. ER-Tracker Red (Cat E34250) was purchased from Life Technologies. Live cells were incubated with 1 μ M ER Tracker on DMEM with 10% FBS for 30 minutes. Cells were washed twice in PBS, re-suspended in PBS with 5% serum, passed through a cell strainer, and analyzed on an Accuri C6 flow cytometer under FL-3. Data analysis was performed using FlowJo software.

Transmission electron microscopy

Cells were fixed with 2.5% glutaraldehyde, 2.0% paraformaldehyde in 0.1M sodium cacodylate buffer, pH7.4, overnight at 4°C. After subsequent buffer washes, the samples were post-fixed in 2.0% osmium tetroxide for 1 hour at room temperature, and then washed again in buffer followed by distilled water. After dehydration through a graded ethanol series, the tissue was infiltrated and embedded in EMbed-812 (Electron Microscopy Sciences, Fort Washington, PA). Thin sections were stained with uranyl acetate and lead citrate and examined with a JEOL 1010 electron microscope fitted with a Hamamatsu digital camera and AMT Advantage image capture software.

PPRE reporter assay

The PPRE X3-TK-luc plasmid was purchased from Addgene (No. 1015). 30,000 cells were seeded into 24 well plates and transfected with 1 μ g of PPRE X3-TK-luc and 100ng of Renilla luciferase plasmids using Fugene 6 (Promega). Luciferase activity was measured two days after transfection using the Dual Luciferase assay kit (Promega).

ATP measurement

ATP luminescence assay system (Cat 6016941) was purchased from Perkin Elmer. 100,000 cells were plated into each well of an opaque 96 well plate and analyzed as described by the manufacturer.

Western blot analysis

Cells were lysed in lysis buffer (40mM HEPES, 2mM EDTA, 10mM pyrophosphate, 10mM glycerophosphate, 1% Triton X-100) containing Roche complete ultra protease/phosphatase inhibitor (Cat 05892791001). Nuclear and cytoplasmic fractionation was performed using the Thermo Scientific NE-PER kit (Cat PI-78833). Isolated proteins were resolved by SDS-PAGE and western blot analysis was performed. All primary antibodies were diluted at 1:1000 in 5% w/v non-fat milk, unless otherwise noted. Blots were incubated with primary antibodies overnight at 4°C. HIF-2 α (Cat NB100-122) and phospho-serine 724 IRE-1 α (Cat NB-100-2323) were purchased from Novus Biologicals. HIF-1 α antibody (Cat 610958) was purchased from BD Biosciences. PLIN2 antibody (Cat ab78920) was purchased from Abcam. β -Actin (1:4000, Cat SC-47778), ATF6 (Cat SC-22799), and ATF4 (1:2000, Cat SC-200) antibodies were purchased from Santa Cruz Biotechnology. Cleaved caspase 3 (Cat 9661), PERK (1:4000, Cat 3192), IRE1 α (Cat 3294), phospho-threonine 389 S6K1 (Cat 9234), S6K1 (Cat 2708), phospho-serine 65 4E-BP1 (Cat 9451), 4E-BP1 (Cat 9452), FASN (Cat 3180), ACC (Cat 3696), HDAC1 (1:4000, Cat 5365), and PPARG (Cat 2435) antibodies were purchased from Cell Signaling Technology. Rabbit polyclonal phospho-

threonine 980 PERK antibody was a gift from Dr. Alan Diehl. Primary antibodies were detected using horseradish peroxidase conjugated secondary antibodies (Cell Signaling Technologies) followed by exposure to ECL (Pierce).

Protein synthesis measurement

Protein synthesis was measured as described (50). Briefly, cells were pulsed with puromycin (30 min, 10 μ g/ml) and chased in puromycin free media (1 hr). Whole cell lysates were subjected to western blot analysis using anti-puromycin antibody (Millipore, Cat MABE343) at 1:20,000.

Metabolomics analysis

Mass spectrometry based metabolomics analysis was performed in conjunction with Metabolon, as previously described (7).

Supplementary Material

Refer to Web version on PubMed Central for supplementary material.

Acknowledgments

The authors thank John Tobias, Ph.D for bioinformatics analyses, Ray Meade for assistance in TEM, and Hongwei Yu for histologic preparations. This work was supported by the Howard Hughes Medical Institute, NIH grant 2-P01-CA104838 to M.C.S, and NIH fellowship 5-F30-CA177106 to B.Q.

References

1. Shen C, Kaelin WG Jr. The VHL/HIF axis in clear cell renal carcinoma. *Seminars in cancer biology*. 2013; 23:18–25. [PubMed: 22705278]
2. Keith B, Johnson RS, Simon MC. HIF1alpha and HIF2alpha: sibling rivalry in hypoxic tumour growth and progression. *Nature reviews Cancer*. 2012; 12:9–22.
3. Shen C, Beroukhi R, Schumacher SE, Zhou J, Chang M, Signoretti S, et al. Genetic and functional studies implicate HIF1alpha as a 14q kidney cancer suppressor gene. *Cancer discovery*. 2011; 1:222–35. [PubMed: 22037472]
4. Gordan JD, Lal P, Dondeti VR, Letrero R, Parekh KN, Oquendo CE, et al. HIF-alpha effects on c-Myc distinguish two subtypes of sporadic VHL-deficient clear cell renal carcinoma. *Cancer cell*. 2008; 14:435–46. [PubMed: 19061835]
5. Purdue MP, Johansson M, Zelenika D, Toro JR, Scelo G, Moore LE, et al. Genome-wide association study of renal cell carcinoma identifies two susceptibility loci on 2p21 and 11q13.3. *Nature genetics*. 2011; 43:60–5. [PubMed: 21131975]
6. Schodel J, Bardella C, Sciesielski LK, Brown JM, Pugh CW, Buckle V, et al. Common genetic variants at the 11q13.3 renal cancer susceptibility locus influence binding of HIF to an enhancer of cyclin D1 expression. *Nature genetics*. 2012; 44:420–5. S1–2. [PubMed: 22406644]
7. Li B, Qiu B, Lee DS, Walton ZE, Ochocki JD, Mathew LK, et al. Fructose-1,6-bisphosphatase opposes renal carcinoma progression. *Nature*. 2014; 513:251–5. [PubMed: 25043030]
8. Walther TC, Farese RV Jr. Lipid droplets and cellular lipid metabolism. *Annual review of biochemistry*. 2012; 81:687–714.
9. Wilfling F, Wang H, Haas JT, Kraemer N, Gould TJ, Uchida A, et al. Triacylglycerol synthesis enzymes mediate lipid droplet growth by relocalizing from the ER to lipid droplets. *Developmental cell*. 2013; 24:384–99. [PubMed: 23415954]

10. Greenberg AS, Coleman RA, Kraemer FB, McManaman JL, Obin MS, Puri V, et al. The role of lipid droplets in metabolic disease in rodents and humans. *The Journal of clinical investigation*. 2011; 121:2102–10. [PubMed: 21633178]
11. Rankin EB, Rha J, Selak MA, Unger TL, Keith B, Liu Q, et al. Hypoxia-inducible factor 2 regulates hepatic lipid metabolism. *Molecular and cellular biology*. 2009; 29:4527–38. [PubMed: 19528226]
12. Hu CJ, Wang LY, Chodosh LA, Keith B, Simon MC. Differential roles of hypoxia-inducible factor 1alpha (HIF-1alpha) and HIF-2alpha in hypoxic gene regulation. *Molecular and cellular biology*. 2003; 23:9361–74. [PubMed: 14645546]
13. Young RM, Ackerman D, Quinn ZL, Mancuso A, Gruber M, Liu L, et al. Dysregulated mTORC1 renders cells critically dependent on desaturated lipids for survival under tumor-like stress. *Genes & development*. 2013; 27:1115–31. [PubMed: 23699409]
14. Ackerman D, Simon MC. Hypoxia, lipids, and cancer: surviving the harsh tumor microenvironment. *Trends in cell biology*. 2014; 24:472–8. [PubMed: 24985940]
15. Volmer R, van der Ploeg K, Ron D. Membrane lipid saturation activates endoplasmic reticulum unfolded protein response transducers through their transmembrane domains. *Proceedings of the National Academy of Sciences of the United States of America*. 2013; 110:4628–33. [PubMed: 23487760]
16. Walter P, Ron D. The unfolded protein response: from stress pathway to homeostatic regulation. *Science*. 2011; 334:1081–6. [PubMed: 22116877]
17. Obeng EA, Carlson LM, Gutman DM, Harrington WJ Jr, Lee KP, Boise LH. Proteasome inhibitors induce a terminal unfolded protein response in multiple myeloma cells. *Blood*. 2006; 107:4907–16. [PubMed: 16507771]
18. Cancer Genome Atlas Research N. Comprehensive molecular characterization of clear cell renal cell carcinoma. *Nature*. 2013; 499:43–9. [PubMed: 23792563]
19. Sun Z, Miller RA, Patel RT, Chen J, Dhir R, Wang H, et al. Hepatic Hdac3 promotes gluconeogenesis by repressing lipid synthesis and sequestration. *Nature medicine*. 2012; 18:934–42.
20. Imai Y, Boyle S, Varela GM, Caron E, Yin X, Dhir R, et al. Effects of perilipin 2 antisense oligonucleotide treatment on hepatic lipid metabolism and gene expression. *Physiological genomics*. 2012; 44:1125–31. [PubMed: 23012396]
21. Imamura M, Inoguchi T, Ikuyama S, Taniguchi S, Kobayashi K, Nakashima N, et al. ADRP stimulates lipid accumulation and lipid droplet formation in murine fibroblasts. *American journal of physiology Endocrinology and metabolism*. 2002; 283:E775–83. [PubMed: 12217895]
22. Kim WY, Safran M, Buckley MR, Ebert BL, Glickman J, Bosenberg M, et al. Failure to prolyl hydroxylate hypoxia-inducible factor alpha phenocopies VHL inactivation in vivo. *The EMBO journal*. 2006; 25:4650–62. [PubMed: 16977322]
23. Jones J, Otu H, Spentzos D, Kolia S, Inan M, Beecken WD, et al. Gene signatures of progression and metastasis in renal cell cancer. *Clinical cancer research : an official journal of the American Association for Cancer Research*. 2005; 11:5730–9. [PubMed: 16115910]
24. Inoue K, Kawahito Y, Tsubouchi Y, Kohno M, Yoshimura R, Yoshikawa T, et al. Expression of peroxisome proliferator-activated receptor gamma in renal cell carcinoma and growth inhibition by its agonists. *Biochemical and biophysical research communications*. 2001; 287:727–32. [PubMed: 11563856]
25. Bensaad K, Favaro E, Lewis CA, Peck B, Lord S, Collins JM, et al. Fatty Acid Uptake and Lipid Storage Induced by HIF-1alpha Contribute to Cell Growth and Survival after Hypoxia-Reoxygenation. *Cell reports*. 2014; 9:349–65. [PubMed: 25263561]
26. Listenberger LL, Han X, Lewis SE, Cases S, Farese RV Jr, Ory DS, et al. Triglyceride accumulation protects against fatty acid-induced lipotoxicity. *Proceedings of the National Academy of Sciences of the United States of America*. 2003; 100:3077–82. [PubMed: 12629214]
27. Osłowski CM, Urano F. Measuring ER stress and the unfolded protein response using mammalian tissue culture system. *Methods in enzymology*. 2011; 490:71–92. [PubMed: 21266244]

28. Atkins C, Liu Q, Minthorn E, Zhang SY, Figueroa DJ, Moss K, et al. Characterization of a novel PERK kinase inhibitor with antitumor and antiangiogenic activity. *Cancer research*. 2013; 73:1993–2002. [PubMed: 23333938]
29. Cross BC, Bond PJ, Sadowski PG, Jha BK, Zak J, Goodman JM, et al. The molecular basis for selective inhibition of unconventional mRNA splicing by an IRE1-binding small molecule. *Proceedings of the National Academy of Sciences of the United States of America*. 2012; 109:E869–78. [PubMed: 22315414]
30. Chang BH, Li L, Paul A, Taniguchi S, Nannegari V, Heird WC, et al. Protection against fatty liver but normal adipogenesis in mice lacking adipose differentiation-related protein. *Molecular and cellular biology*. 2006; 26:1063–76. [PubMed: 16428458]
31. Son SH, Goo YH, Chang BH, Paul A. Perilipin 2 (PLIN2)-deficiency does not increase cholesterol-induced toxicity in macrophages. *PloS one*. 2012; 7:e33063. [PubMed: 22427949]
32. Roschinger W, Muntau AC, Duran M, Dorland L, LJJ, Wanders RJ, et al. Carnitine-acylcarnitine translocase deficiency: metabolic consequences of an impaired mitochondrial carnitine cycle. *Clinica chimica acta; international journal of clinical chemistry*. 2000; 298:55–68.
33. Walter KM, Schonenberger MJ, Trotschmuller M, Horn M, Elsasser HP, Moser AB, et al. Hif-2alpha promotes degradation of Mammalian peroxisomes by selective autophagy. *Cell metabolism*. 2014; 20:882–97. [PubMed: 25440060]
34. Haddad AQ, Kapur P, Singla N, Raman JD, Then MT, Nuhn P, et al. Validation of mammalian target of rapamycin biomarker panel in patients with clear cell renal cell carcinoma. *Cancer*. 2015; 121:43–50. [PubMed: 25186283]
35. Peterson TR, Sengupta SS, Harris TE, Carmack AE, Kang SA, Balderas E, et al. mTOR complex 1 regulates lipin 1 localization to control the SREBP pathway. *Cell*. 2011; 146:408–20. [PubMed: 21816276]
36. Duvel K, Yecies JL, Menon S, Raman P, Lipovsky AI, Souza AL, et al. Activation of a metabolic gene regulatory network downstream of mTOR complex 1. *Molecular cell*. 2010; 39:171–83. [PubMed: 20670887]
37. Kammoun HL, Chabanon H, Hainault I, Luquet S, Magnan C, Koike T, et al. GRP78 expression inhibits insulin and ER stress-induced SREBP-1c activation and reduces hepatic steatosis in mice. *The Journal of clinical investigation*. 2009; 119:1201–15. [PubMed: 19363290]
38. Ling SC, Lau EK, Al-Shabeeb A, Nikolic A, Catalano A, Iland H, et al. Response of myeloma to the proteasome inhibitor bortezomib is correlated with the unfolded protein response regulator XBP-1. *Haematologica*. 2012; 97:64–72. [PubMed: 21993678]
39. Kawabata S, Gills JJ, Mercado-Matos JR, Lopiccolo J, Wilson W 3rd, Hollander MC, et al. Synergistic effects of nelfinavir and bortezomib on proteotoxic death of NSCLC and multiple myeloma cells. *Cell death & disease*. 2012; 3:e353. [PubMed: 22825471]
40. Fels DR, Ye J, Segan AT, Kridel SJ, Spiotto M, Olson M, et al. Preferential cytotoxicity of bortezomib toward hypoxic tumor cells via overactivation of endoplasmic reticulum stress pathways. *Cancer research*. 2008; 68:9323–30. [PubMed: 19010906]
41. Sztalryd C, Bell M, Lu X, Mertz P, Hickenbottom S, Chang BH, et al. Functional compensation for adipose differentiation-related protein (ADFP) by Tip47 in an ADFP null embryonic cell line. *The Journal of biological chemistry*. 2006; 281:34341–8. [PubMed: 16968708]
42. Hart LS, Cunningham JT, Datta T, Dey S, Tameire F, Lehman SL, et al. ER stress-mediated autophagy promotes Myc-dependent transformation and tumor growth. *The Journal of clinical investigation*. 2012; 122:4621–34. [PubMed: 23143306]
43. Commisso C, Davidson SM, Soydaner-Azeloglu RG, Parker SJ, Kamphorst JJ, Hackett S, et al. Macropinocytosis of protein is an amino acid supply route in Ras-transformed cells. *Nature*. 2013; 497:633–7. [PubMed: 23665962]
44. Kamphorst JJ, Cross JR, Fan J, de Stanchina E, Mathew R, White EP, et al. Hypoxic and Ras-transformed cells support growth by scavenging unsaturated fatty acids from lysophospholipids. *Proceedings of the National Academy of Sciences of the United States of America*. 2013; 110:8882–7. [PubMed: 23671091]

45. Elorza A, Soro-Arnaiz I, Melendez-Rodriguez F, Rodriguez-Vaello V, Marsboom G, de Carcer G, et al. HIF2alpha acts as an mTORC1 activator through the amino acid carrier SLC7A5. *Molecular cell*. 2012; 48:681–91. [PubMed: 23103253]
46. Yue S, Li J, Lee SY, Lee HJ, Shao T, Song B, et al. Cholesteryl ester accumulation induced by PTEN loss and PI3K/AKT activation underlies human prostate cancer aggressiveness. *Cell metabolism*. 2014; 19:393–406. [PubMed: 24606897]
47. Bozza PT, Viola JP. Lipid droplets in inflammation and cancer. *Prostaglandins, leukotrienes, and essential fatty acids*. 2010; 82:243–50.
48. Fu S, Yang L, Li P, Hofmann O, Dicker L, Hide W, et al. Aberrant lipid metabolism disrupts calcium homeostasis causing liver endoplasmic reticulum stress in obesity. *Nature*. 2011; 473:528–31. [PubMed: 21532591]
49. Kondagunta GV, Drucker B, Schwartz L, Bacik J, Marion S, Russo P, et al. Phase II trial of bortezomib for patients with advanced renal cell carcinoma. *Journal of clinical oncology : official journal of the American Society of Clinical Oncology*. 2004; 22:3720–5. [PubMed: 15365068]
50. Schmidt EK, Clavarino G, Ceppi M, Pierre P. SUnSET, a nonradioactive method to monitor protein synthesis. *Nature methods*. 2009; 6:275–7. [PubMed: 19305406]

Significance

We demonstrate that HIF-2 α promotes lipid storage, ER homeostasis, and cell viability in ccRCC via upregulation of the LD coat protein PLIN2, revealing a novel function for the well documented “clear cell” phenotype and identifying ER stress as a targetable vulnerability created by HIF-2 α /PLIN2 suppression in this common renal malignancy.

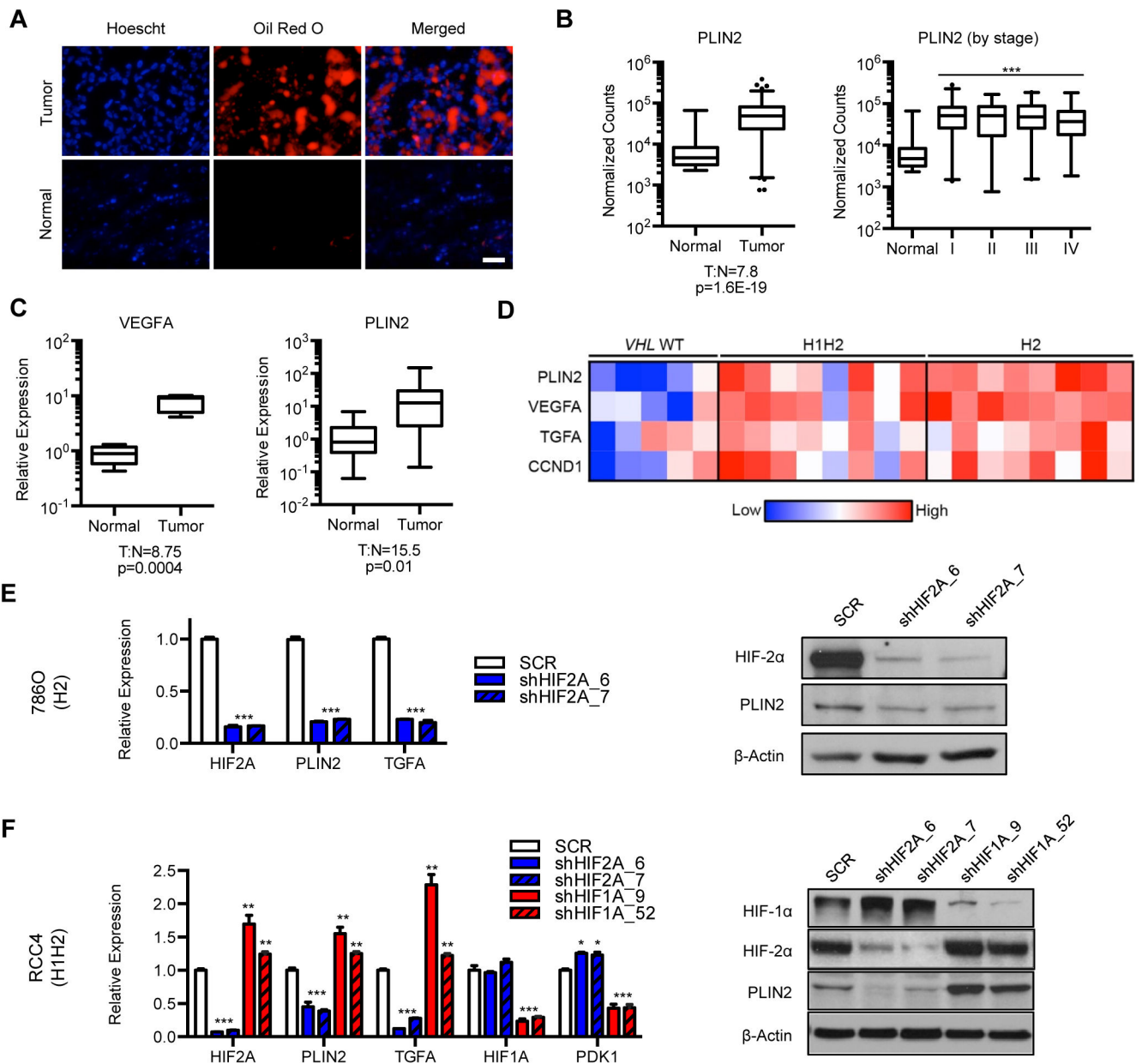


Figure 1. HIF-2 α promotes expression of the lipid droplet coat protein PLIN2 in ccRCC

A) Oil red O staining of matched primary ccRCC and normal kidney samples. Scale bar = 50 μ m.

B) Normalized RNA-seq reads of *PLIN2* in ccRCC (n=480) and normal kidney (n=69) samples. Tumors were also analyzed for *PLIN2* expression according to tumor stage. RNA-seq data was obtained from The Cancer Genome Atlas (TCGA), and p-values determined by DEseq. Whiskers denote the 1st and 99th percentiles.

C) Quantitative RT-PCR (qRT-PCR) analysis of *VEGFA* and *PLIN2* in matched ccRCC (n=10) and normal kidney (n=10) samples obtained from the Cooperative Human Tissue Network (CHTN). Whiskers denote the 1st and 99th percentiles.

D) Microarray analysis of primary ccRCC samples that have been previously classified by *VHL* genotyping and HIF- α immunohistochemical staining to reveal 3 sub-types: *VHL* WT (no HIF-1 α or HIF-2 α staining and confirmed WT sequence at *VHL* locus, n=5), H1H2 (HIF-1 α and HIF-2 α staining, n=8), and H2 (HIF-2 α staining only, n=8). Expression of *PLIN2* and multiple known HIF-2 α target genes in ccRCC are shown. *PLIN2* mRNA was elevated in both H1H2 (9.7 fold overexpression, p=2.6E-4) and H2 (16.7 fold overexpression, p=2.5E-6) tumors compared to *VHL* WT samples. p-values determined by ANOVA.

E) 786-O (H2) ccRCC cells were transduced with two independent shRNAs against *HIF2A* (shHIF2A_6 and 7) or a SCR control. qRT-PCR and western blot analysis of *PLIN2* are shown. *TGFA* is included as a positive control for HIF-2 α suppression.

F) RCC4 (H1H2) ccRCC cells were transduced with two independent shRNAs against HIF-1 α (shHIF1A_9 and 52), HIF-2 α (shHIF2A_6 and 7), or a SCR control. qRT-PCR and western blot for *PLIN2* is shown. *TGFA* and *PDK1* are included as positive controls for HIF-2 α and HIF-1 α suppression, respectively. Data are representative of three independent experiments. Unless otherwise noted, p-values were determined by student's t-test. * p<0.05, ** p<0.01, *** p<0.001. For qRT-PCR, *TBP* and *ACTB* were utilized as endogenous control genes and relative mRNA expression was determined by normalizing to expression in SCR samples. Error bars denote standard error of the mean (SEM).

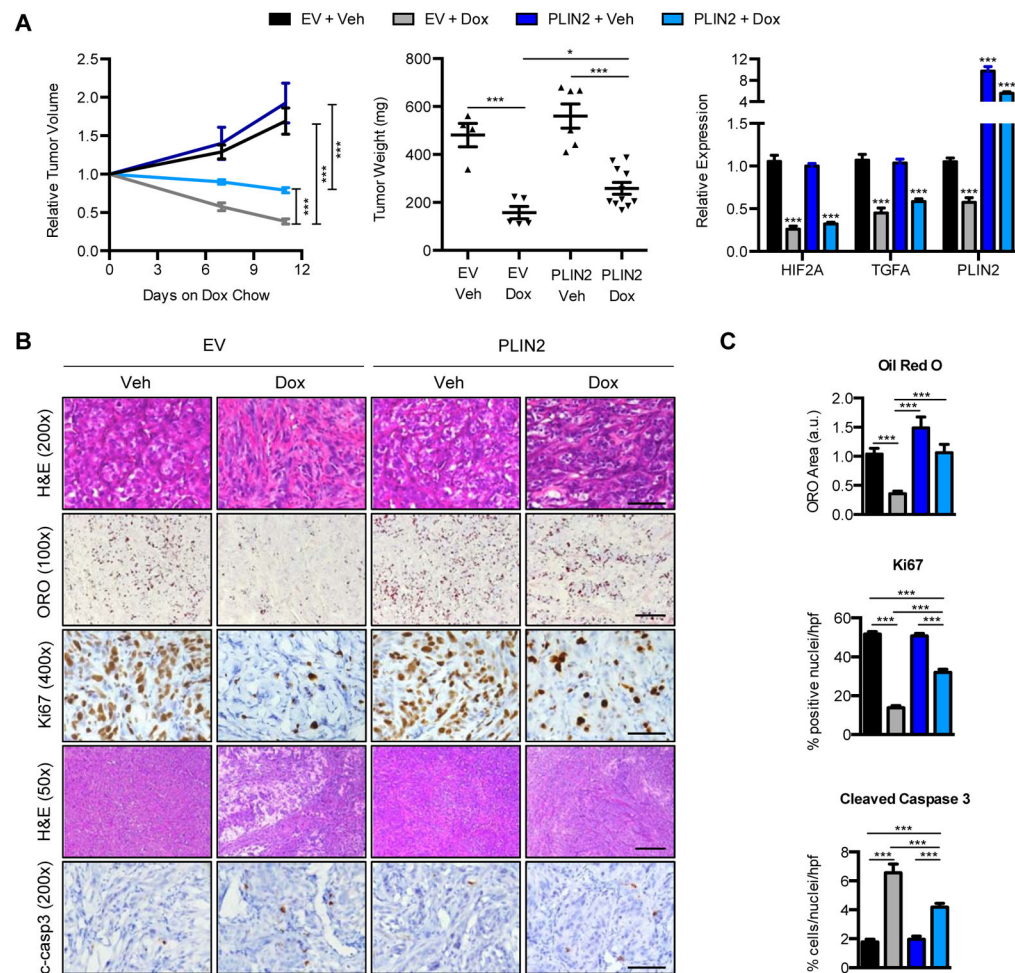


Figure 2. HIF-2 α dependent *PLIN2* expression and lipid storage promotes xenograft tumor growth

A) Sub-cutaneous tumors of 786-O cells expressing Dox-inducible shHIF2A_7, along with either empty vector or exogenous *PLIN2*, were generated in NIH-III nude mice. Once tumor volume reached 300mm³, a cohort received Dox-chow (625 mg/kg). Relative tumor volume was monitored until 11 days of Dox treatment (left). Tumor weights at harvest were determined (center), and qRT-PCR analysis for *HIF-2 α* , *TGFA*, and *PLIN2* was performed (right). EV Veh, n=4; EV Dox, n=5; PLIN2 Veh n=6; PLIN2 Dox, n=9. For qRT-PCR, *TBP* and *ACTB* were utilized as endogenous control genes and relative mRNA expression was determined by normalizing to expression in EV Veh samples.

B) Histological analysis of tumors is shown. The indicated stains were performed on sections obtained from tumors described in (A). Scale bars: 50x=400 μ m, 100x=200 μ m, 200x=100 μ m, 400x=50 μ m.

C) Oil red O area per field was determined using Image J. Percentage of cells per field that exhibited nuclear Ki67 or cleaved caspase 3 expression is shown. For each graph, 30 fields per tumor type were quantified. p-values were determined by two-way ANOVA with Bonferroni correction. * p<0.05, ** p<0.01, *** p<0.001. Error bars denote SEM.

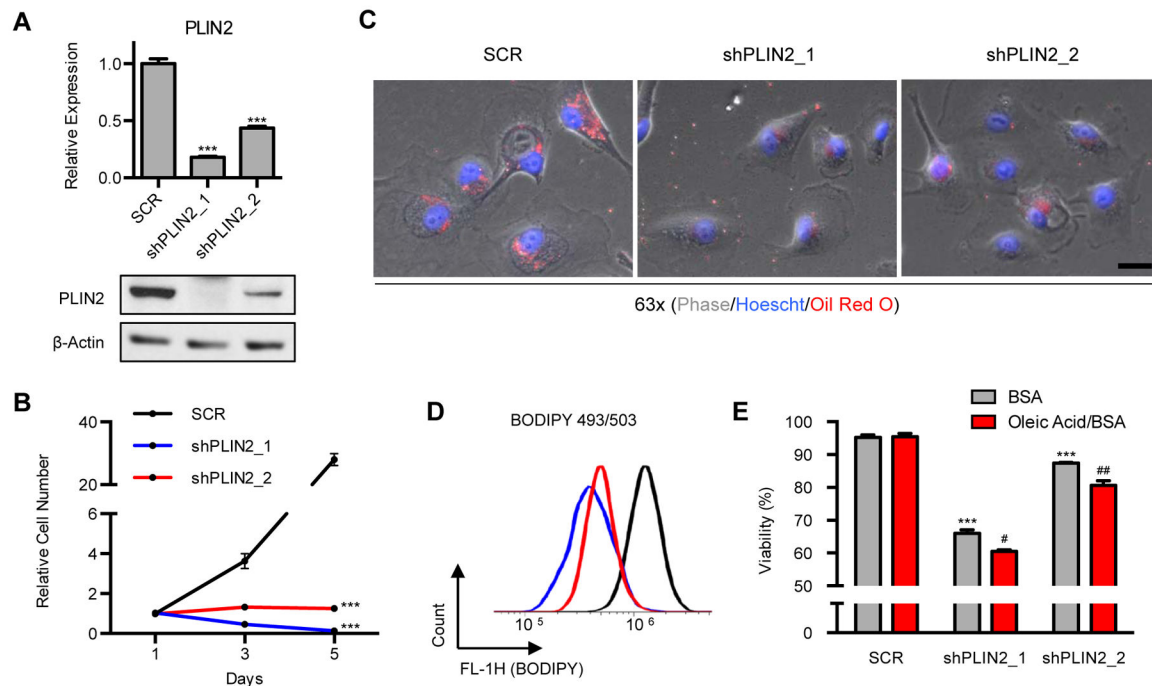


Figure 3. PLIN2 is required for lipid storage and cell viability

A) 786-O ccRCC cells were transduced with two independent shRNAs against *PLIN2* (shPLIN2_1, shPLIN2_2) or a SCR control. qRT-PCR and western blot analysis were performed on day 3 post shRNA transduction to assess for *PLIN2* suppression. For qRT-PCR, *TBP* and *ACTB* were utilized as endogenous control genes and relative mRNA expression was determined by normalizing to expression in SCR samples. p-values were determined by student's t-test. *** $p < 0.001$.

B) Growth curves for cells described in (A). Day 1 of growth curve corresponds to day 3 post transduction.

C) Oil Red O staining of cells described in (A) was performed on day 3 post transduction. Scale bar = 50 μ m.

D) Live cells described in (A) were stained with BODIPY 493/503 (2 μ g/ml) and fluorescence was measured by flow cytometry. A histogram of BODIPY 493/503 fluorescence is shown.

E) Beginning on day 3 post transduction, cells from (A) were treated with BSA alone or BSA conjugated with oleic acid (30 μ M). Viability was determined by annexin/PI staining after 24 hours of treatment. Data are representative of three independent experiments. p-values were determined by two-way ANOVA with Bonferroni correction. Asterisks denote comparison with SCR BSA. *** $p < 0.001$. Pound signs denote comparison of Oleic Acid with BSA treated conditions within each cell line. # $p < 0.05$, ## $p < 0.01$. Error bars denote SEM.

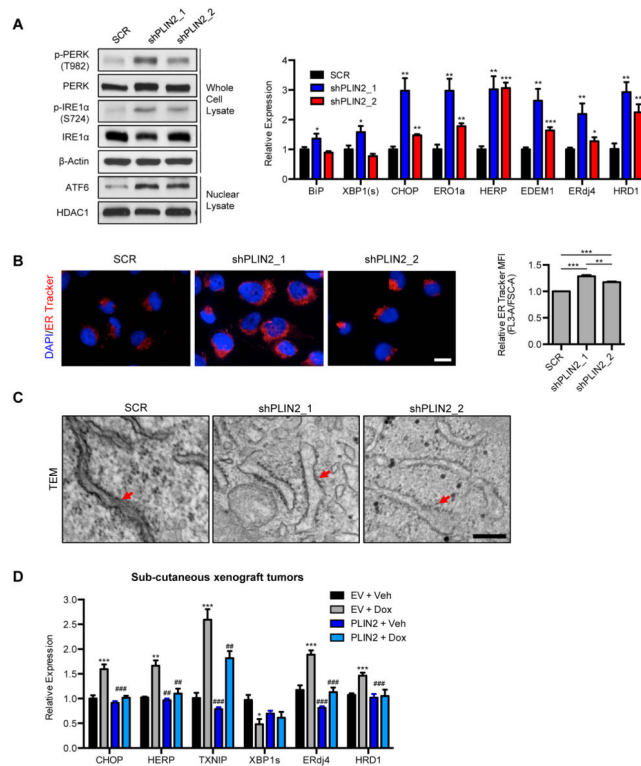


Figure 4. PLIN2 dependent lipid storage promotes ER homeostasis in ccRCC

A) Western blot for UPR sensors was performed in 786-O cells expressing independent shRNAs against *PLIN2* (shPLIN2_1, shPLIN2_2) or a SCR control (left, day 3 post transduction). Corresponding qRT-PCR analysis of UPR target genes is shown (right, day 4 post transduction). Data are representative of three independent experiments. p-values were determined by student's t-test.

B) ER Tracker Red (500 nM) staining of live cells described in (A) was performed (day 4 post transduction). Representative images (left) and quantification of ER Tracker fluorescence are shown (right). Fluorescence was normalized to forward scatter for each event to account for differences in cell size. Scale bar = 50 μ m. p-values were determined by student's t-test.

C) Transmission electron microscopy of control and PLIN2 depleted cells is shown (day 4 post transduction). Red arrows denote rough ER. Scale bar=200 nm.

D) qRT-PCR of xenograft tumor RNA assessing expression of UPR target genes. p-values were determined by two-way ANOVA with Bonferroni correction. Asterisks denote comparison with EV Veh. * p<0.05, ** p<0.01, *** p<0.001. Pound signs denote comparison with EV Dox. ## p<0.01, ### p<0.001. Error bars denote SEM.

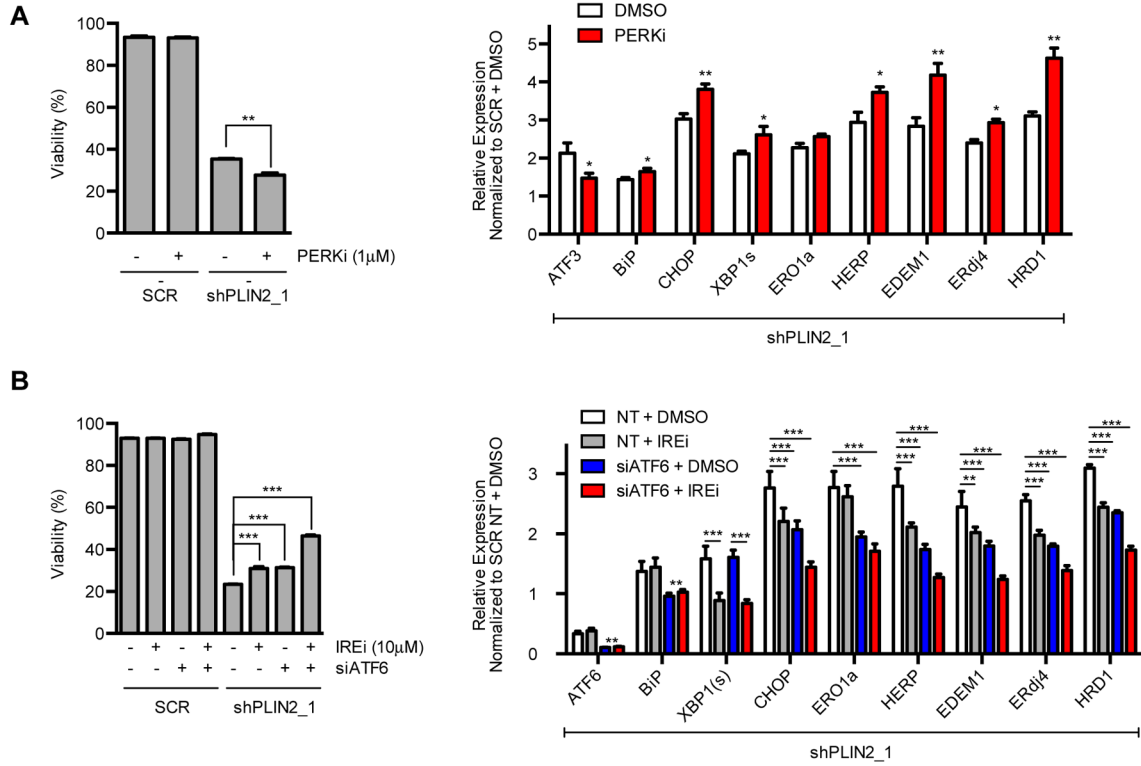


Figure 5. Unfolded protein response promotes cell death upon PLIN2 depletion

A) 786-O cells expressing shPLIN2_1 or SCR control were treated with PERK inhibitor (1 μ M) or DMSO vehicle beginning on day 3 post transduction. Cell viability was determined by annexin/PI staining after 48 hours of drug treatment and qRT-PCR analysis of UPR target gene expression was performed after 24 hours of drug treatment. For qRT-PCR, *TBP* and *ACTB* were utilized as endogenous control genes and relative mRNA expression was determined by normalizing to expression in SCR samples. Data are representative of three independent experiments. p-values were determined by student's t-test. * p<0.05, ** p<0.01, *** p<0.001.

B) 786-O cells expressing shPLIN2_1 or SCR shRNA were transfected with non-targeting (NT) or ATF6 directed siRNA (day 2 post transduction) and subsequently treated with IRE-1 α inhibitor (10 μ M) or DMSO vehicle (day 3 post transduction). Cell viability was determined by annexin/PI staining after 48 hours of drug treatment (left) and qRT-PCR analysis of UPR target gene expression was performed after 24 hours of drug treatment (right). Data are representative of three independent experiments. p-values were determined by two-way ANOVA with Bonferroni correction. ** p<0.01, *** p<0.001. Error bars denote SEM.

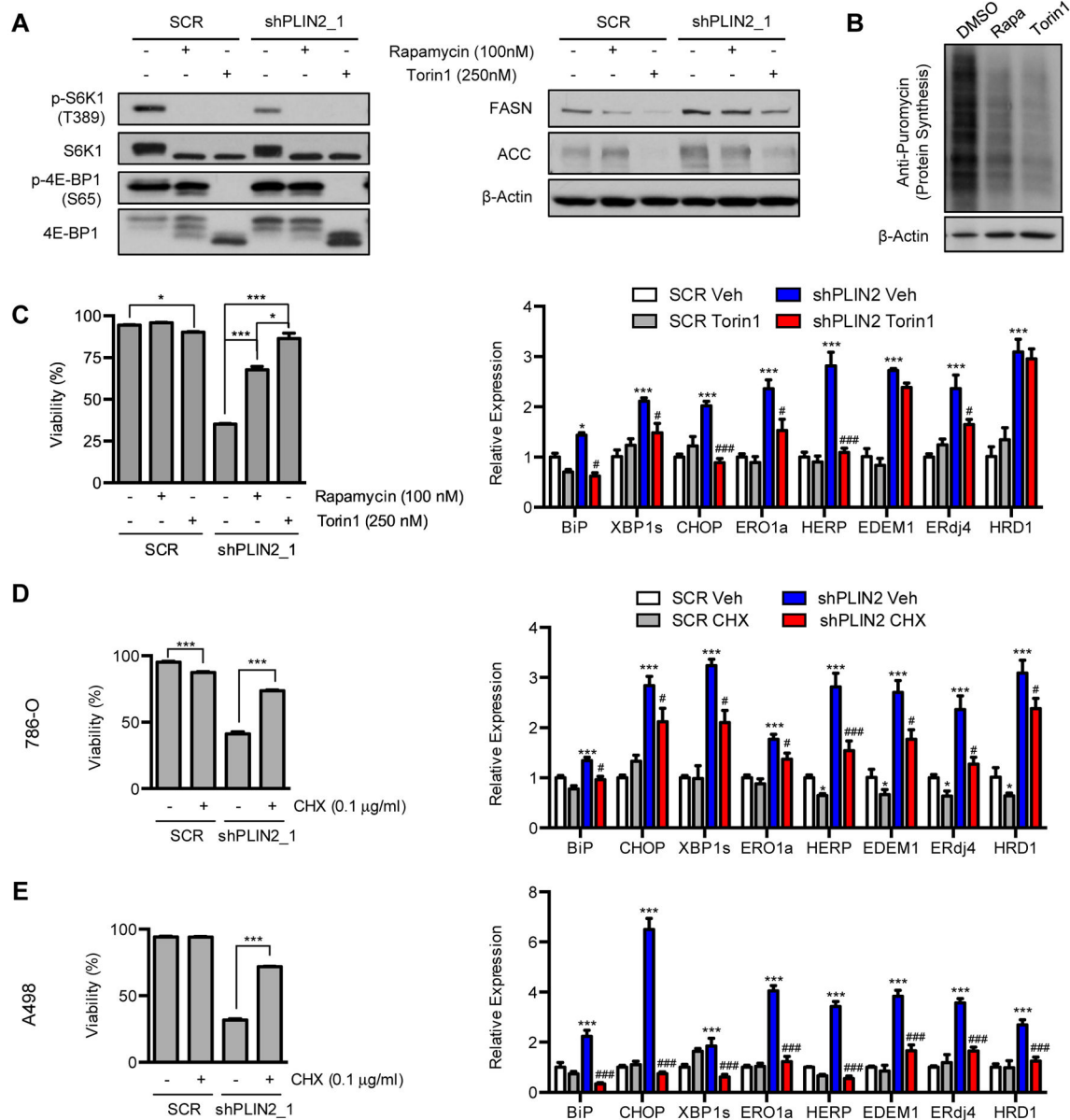


Figure 6. Suppression of protein synthesis ameliorates ER stress and cell death upon PLIN2 depletion

A) 786-O cells expressing shPLIN2_1 or SCR control were treated with rapamycin (100 nM) or Torin1 (250 nM) for 48 hours. Western blot analysis of direct targets of mTORC1 kinase (left) and mTORC1 regulated fatty acid synthesis enzymes (right) are shown.

B) Protein synthesis activity was measured in 786-O cells treated with rapamycin, Torin1, or DMSO vehicle for 48 hours. Cells were pulsed with puromycin (30 min, 10μg/ml) and chased in puromycin free media (1 hr) to allow puromycin incorporation into nascent peptides. Whole cell lysates were subjected to western blot analysis using an anti-puromycin antibody (clone 12D10).

C) 786-O cells expressing shPLIN2_1 or SCR control were treated with rapamycin, Torin1, or DMSO vehicle starting on day 3 post transduction and cell viability was determined by

annexin/PI staining after 48 hours of drug treatment (left). qRT-PCR comparing UPR target gene expression in cells treated with Torin1 was performed after 24 hours of drug treatment. D) 786-O cells expressing shPLIN2_1 or SCR shRNA were treated with cycloheximide or DMSO vehicle starting on day 3 post transduction and cell viability was determined by annexin/PI staining after 48 hours of drug treatment (left). qRT-PCR for UPR target genes was performed after 24 hours of drug treatment (right).

E) A498 cells were treated and analyzed as described in (D). Data are representative of three independent experiments. p-values were determined by student's t-test for annexin/PI assays and two-way ANOVA with Bonferroni correction for qRT-PCR. For qRT-PCR, *TBP* and *ACTB* were utilized as endogenous control genes and relative mRNA expression was determined by normalizing to expression in SCR Veh samples. Asterisks denote statistical comparison with SCR Veh. * p<0.05, *** p<0.001. Pound signs denote statistical comparison with shPLIN2 Veh. # p<0.05, ### p<0.001. Error bars denote SEM.

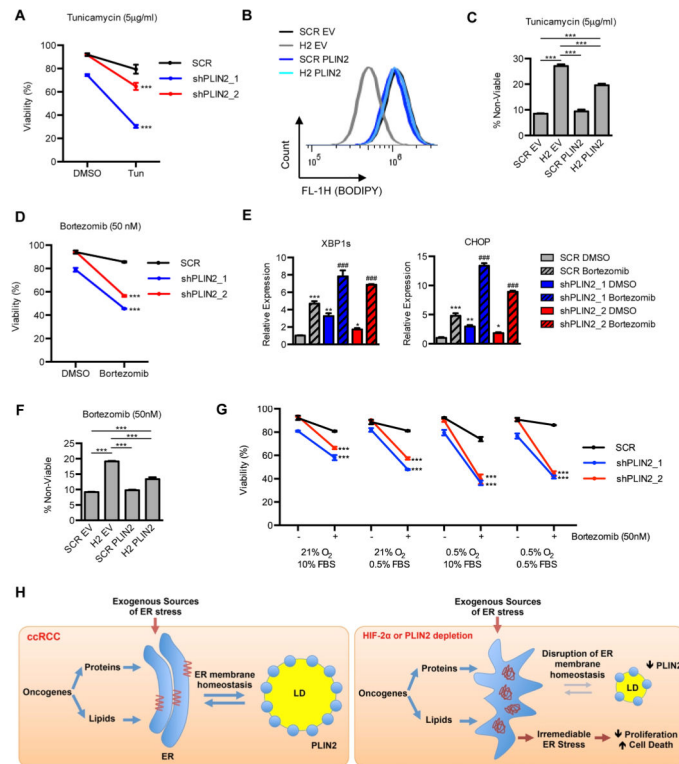


Figure 7. HIF-2 α /PLIN2 dependent lipid storage protects ccRCC cells against pharmacological ER stress

A) A498 cells expressing shPLIN2_1, shPLIN2_2, or SCR control were treated with tunicamycin or DMSO at 2 days post transduction. Cell viability was determined by annexin/PI staining after 48 hours of drug treatment. Asterisks denote statistical comparison of viability under tunicamycin treatment. Tunicamycin-induced reduction in viability was significantly different between shPLIN2 and SCR cells: shPLIN2_1 vs SCR, $p < 0.01$; shPLIN2_2 vs SCR, $p < 0.01$.

B) A498 cells expressing shHIF2A_7 or SCR control, along with either exogenous PLIN2 or an empty vector (EV), were stained with BODIPY 493/503 (2 μ g/ml). Histograms indicating BODIPY fluorescence was generated by flow cytometry.

C) Cells described in (B) were treated with tunicamycin or DMSO control for 48 hours and viability was determined by annexin/PI staining.

D) A498 cells expressing shPLIN2_1, shPLIN2_2, or SCR control were treated with Bortezomib or DMSO at 3 days post transduction. Cell viability was determined by annexin/PI staining after 24 hours of drug treatment. Asterisks denote statistical comparison of viability under Bortezomib treatment. Bortezomib-induced reduction in viability was significantly different between shPLIN2 and SCR cells: shPLIN2_1 vs SCR, $p < 0.001$ shPLIN2_2 vs SCR, $p < 0.001$

E) *XBPs* and *CHOP* expression in cells from (D) was determined by qRT-PCR. Asterisks denote comparison with SCR DMSO. Pound signs denote comparison with SCR Bortezomib. For qRT-PCR, *TBP* and *ACTB* were utilized as endogenous control genes and relative mRNA expression was determined by normalizing to expression in SCR DMSO samples.

F) Cells described in (B) were treated with Bortezomib or DMSO control for 24 hours and viability was determined by annexin/PI staining.

G) A498 cells expressing shPLIN2_1, shPLIN2_2, or SCR control were treated with Bortezomib or DMSO at 3 days post transduction and incubated under the designated serum and oxygen conditions. Cell viability was determined by annexin/PI staining after 24 hours of drug treatment. Astericks denote comparison with SCR Bortezomib. Under each serum and oxygen condition, Bortezomib-induced reduction in viability was significantly different between shPLIN2 and SCR cells: shPLIN2_1 vs SCR, $p < 0.001$ shPLIN2_2 vs SCR, $p < 0.001$

H) Proposed model illustrating the protective function of HIF-2 α dependent PLIN2 expression and lipid storage against ER stress in ccRCC cells. Data are representative of three independent experiments. p-values were determined by two-way ANOVA with Bonferroni correction. * $p < 0.05$, ** $p < 0.01$, *** $p < 0.001$. ### $p < 0.001$. Error bars denote SEM.